

# An expanded genome-scale model of *Escherichia coli* K-12 (iJR904 GSM/GPR)

Jennifer L Reed\*, Thuy D Vo\*, Christophe H Schilling<sup>†</sup> and Bernhard O Palsson\*

Addresses: \*Department of Bioengineering, University of California, San Diego, Gilman Drive, La Jolla, CA 92092, USA. <sup>†</sup>Genomatica, Inc., Morehouse Drive, San Diego, CA 92121, USA.

Correspondence: Bernhard O Palsson. E-mail: bpalsson@be-research.ucsd.edu

Published: 28 August 2003

*Genome Biology* 2003, 4:R54

The electronic version of this article is the complete one and can be found online at <http://genomebiology.com/2003/4/9/R54>

Received: 9 May 2003

Revised: 11 July 2003

Accepted: 18 July 2003

© 2003 Reed et al.; licensee BioMed Central Ltd. This is an Open Access article: verbatim copying and redistribution of this article are permitted in all media for any purpose, provided this notice is preserved along with the article's original URL.

## Abstract

**Background:** Diverse datasets, including genomic, transcriptomic, proteomic and metabolomic data, are becoming readily available for specific organisms. There is currently a need to integrate these datasets within an *in silico* modeling framework. Constraint-based models of *Escherichia coli* K-12 MG1655 have been developed and used to study the bacterium's metabolism and phenotypic behavior. The most comprehensive *E. coli* model to date (*E. coli* iJE660a GSM) accounts for 660 genes and includes 627 unique biochemical reactions.

**Results:** An expanded genome-scale metabolic model of *E. coli* (iJR904 GSM/GPR) has been reconstructed which includes 904 genes and 931 unique biochemical reactions. The reactions in the expanded model are both elementally and charge balanced. Network gap analysis led to putative assignments for 55 open reading frames (ORFs). Gene to protein to reaction associations (GPR) are now directly included in the model. Comparisons between predictions made by iJR904 and iJE660a models show that they are generally similar but differ under certain circumstances. Analysis of genome-scale proton balancing shows how the flux of protons into and out of the medium is important for maximizing cellular growth.

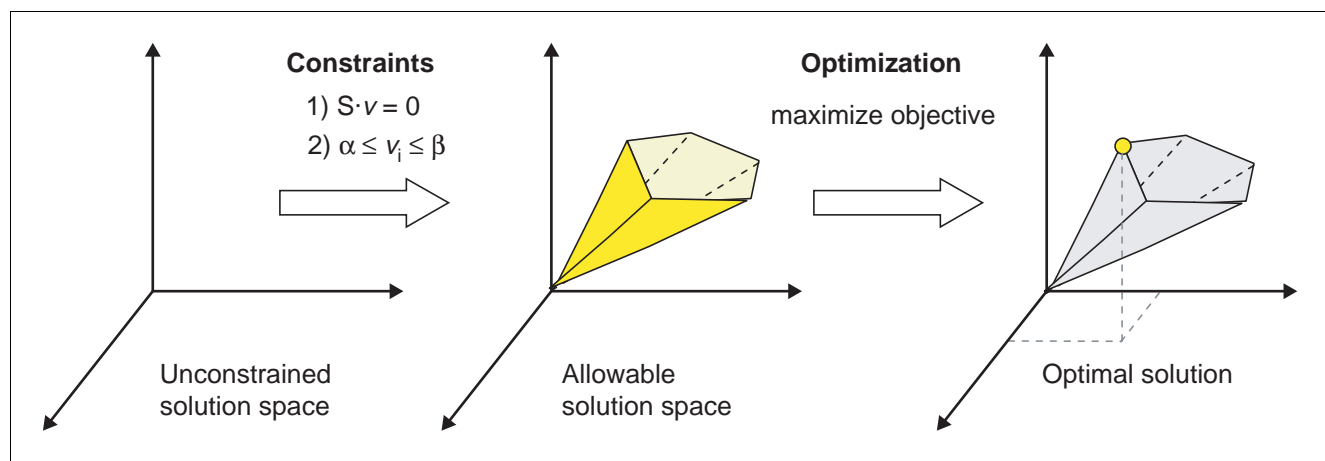
**Conclusions:** *E. coli* iJR904 has improved capabilities over iJE660a. iJR904 is a more complete and chemically accurate description of *E. coli* metabolism than iJE660a. Perhaps most importantly, iJR904 can be used for analyzing and integrating the diverse datasets. iJR904 will help to outline the genotype-phenotype relationship for *E. coli* K-12, as it can account for genomic, transcriptomic, proteomic and fluxomic data simultaneously.

## Background

*Escherichia coli* is perhaps the best characterized and studied bacterium and is of interest industrially, genetically and pathologically. For these reasons, *in silico* modeling efforts have been made to describe and predict its cellular behavior. With the vast amounts of '-omics' data that are being generated, there is a growing need for incorporating and reconciling

heterogeneous datasets, including genomic, transcriptomic, proteomic and metabolomic data [1]. A constraint-based model of *E. coli* metabolism can accomplish this and serve as a model centric database.

In addition to providing the context for various '-omics' data types, constraint-based models provide a framework to

**Figure 1**

Principles of constraint-based modeling. A three-dimensional flux space for a given metabolic network is depicted here. Without any constraints the fluxes can take on any real value. After application of stoichiometric, thermodynamic and enzyme capacity constraints, the possible solutions are confined to a region in the total flux space, termed the allowable solution space. Any point outside of this space violates one or more of the applied constraints. Linear optimization can then be applied to identify a solution in the allowable solution space that maximizes or minimizes a defined objective, for example ATP or biomass production [3-6].

compute cellular functions [2]. This modeling method finds the limits of cellular, biochemical and systemic functions, thereby identifying all allowable solutions. Searches within the allowable solution space can identify solutions of interest, for example a solution that maximizes a particular objective. This approach to genome-scale model building has been reviewed in detail [3-6]. In general, the application of successive constraints (stoichiometric, thermodynamic and enzyme capacity constraints), with respect to the metabolic network, restricts the number of possible solutions. Linear optimization is often used to find a particular solution in the allowable solution space that maximizes a chosen objective function, such as cellular growth (Figure 1). A more detailed description of the constraint-based modeling approach can be found in Materials and methods.

The constraint-based modeling approach has been used to study *E. coli* metabolism for over ten years; the history of such model building efforts has recently been reviewed [7]. The first genome-scale metabolic (GSM) model accounting for 660 gene products (*iJE660* GSM) was reconstructed using genomic information, biochemical data and physiological data [8]. This genome-scale model has been used to perform *in silico* gene deletion studies [8] and to predict both optimal growth behavior [9] and the outcome of adaptive evolution [10].

This paper reports an expansion of *iJE660a* GSM, which itself is a slight modification of the original genome-scale metabolic model (*iJE660* GSM) [8]. Gene to protein to reaction (GPR) associations are included directly in the new model (*iJR904* GSM/GPR). These associations describe the

dependence of reactions on proteins and proteins on genes (Figure 2). The metabolic network described by *iJR904* has also changed; individual reactions are now elementally and charge balanced, and a significant number of new genes and novel reactions have been added to the model. *iJR904* GSM/GPR accounts for over 904 genes and the 931 unique biochemical reactions the encoded proteins carry out. This paper discusses the effects that these additional reactions have on the predictive capabilities of the model and identifies putative ORFs in the genome which could resolve gaps in the metabolic network.

Since computational models of *E. coli* will continue to grow in size and scope [7] it will become important to be able to distinguish between the different models - a naming convention will aid in this effort. The naming convention we chose to use mirrors the one already established for plasmids. The general form of the names of *in silico* strains used is *iXXxxxa* YYY. The 'i' in the name refers to an *in silico* model (that is, a computer model). This 'i' is followed by the initials (XX) of the person who developed the model and then the number of genes (xxx) included in the model. Any letters (a) after the number of genes indicates that slight modifications were made to the model, for instance *iJE660a* is derived from *iJE660*. Further designation of the content and scope of a model are found in YYY; here the acronyms GSM and GPR stand for genome-scale model and gene-protein-reaction associations, respectively. The contents of *iJE660a* and *iJR904* can be found on our website [11], and *iJR904* is also detailed in the additional data files provided with this publication online.

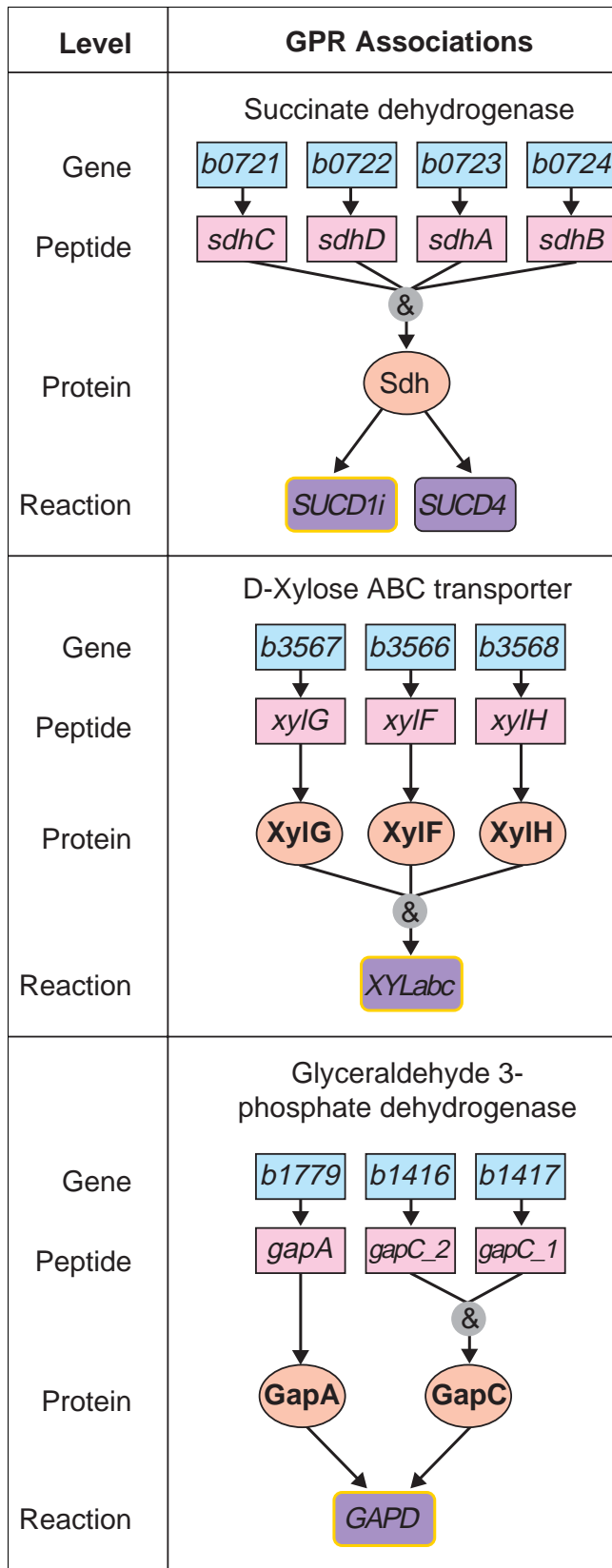


**Figure 2**

Representation of gene to protein to reaction (GPR) associations. Each gene included in the model is associated with at least one reaction. Examples of different types of associations are shown, where the top layer is the gene locus, the second layer is the translated peptide, the third layer is the functional protein and the bottom layer is the reaction (shown as its corresponding abbreviation listed in the additional data file). Subunits (for example, sdhABCD and gapC\_1C\_2) and enzyme complexes (for example, xylFGH) are connected to reactions with '&' associations, indicating that all have to be expressed for the reaction to occur. For sdhABCD, the '&' is shown above the functional protein level, denoting that all of these gene products are needed for the functional enzyme. With xylFGH the '&' association is shown above the reaction level, indicating that the different proteins form a complex that carries out the reaction. Isozymes (for example, gapC\_1C\_2 and gapA) are independent proteins which carry out identical reactions where only one of the isozymes needs to be present for the reaction to occur. Isozymes are shown as two or more arrows leaving different proteins but impinging on the same reaction.

**Results and discussion**

**Properties of the iJR904 metabolic network**

An update on the annotation of the *E. coli* K-12 genome was published in 2001 [12], facilitating the process of updating the genome-scale *in silico* *E. coli* model (*iJE660a* GSM). Genes encoding known or putative enzymes and transporters not included in the *iJE660a* model were further examined. Literature and database searches (LIGAND [13], EcoCyc [14] and TC-DB [15]) on each of the genes provided the biochemical information needed to expand *E. coli* *iJE660a*. The *iJR904* model was built using the software SimPheny™ (Genomatica, San Diego, CA) and accounts for 904 genes with a known locus in the genome, as compared to 660 genes in the previous model.

The metabolic network described by *E. coli* *iJE660a* has expanded in size from 627 unique reactions and 438 metabolites to 931 unique reactions and 625 metabolites in *iJR904*. Complete maps containing all the reactions in the metabolic network are available in the additional data files and can also be downloaded from [11]. The molecular formulae and charges for the metabolites in the model were determined assuming a pH of 7.2. Fifty-eight of the reactions in *iJR904* currently do not have associated genes. A complete list of the reactions can be found in the additional data files. Putative functional gene assignments account for 23 of the added reactions, with the majority of these being putative transporters.

In addition to these new reactions, old reactions were updated to be both elementally and charge balanced by including water and protons as participants in the reactions. Six reactions in *iJR904* are elementally balanced but not charge balanced (Table 1). Five out of the six reactions are imbalanced because they have not been fully characterized biochemically so assumptions had to be made about the participating metabolites; the remaining reaction (abbreviated ADOCBL5) is charge imbalanced since we were unable to

**Table 1****List of charge imbalanced reactions used in *iJR904***

| Abbreviation | Reaction   |
|--------------|--|
| ADOCBLS      | agdpcbi + rdmzbi → adocbl + gmp + h                    |
| AMPMS        | air + h <sub>2</sub> o → 4ampm + (2) for + (4) h       |
| BTS2         | cys-L + dtbt ↔ ala-L + btn + (2) h                     |
| DHNAOT       | dhna + octdp → 2dmmq8 + co <sub>2</sub> + h + ppi      |
| DKMPPD2      | dkmpp + (3) h <sub>2</sub> o → 2kmb + for + (6) h + pi |
| MECDPDH      | 2mecdp + h → h2mb4p + h <sub>2</sub> o                 |

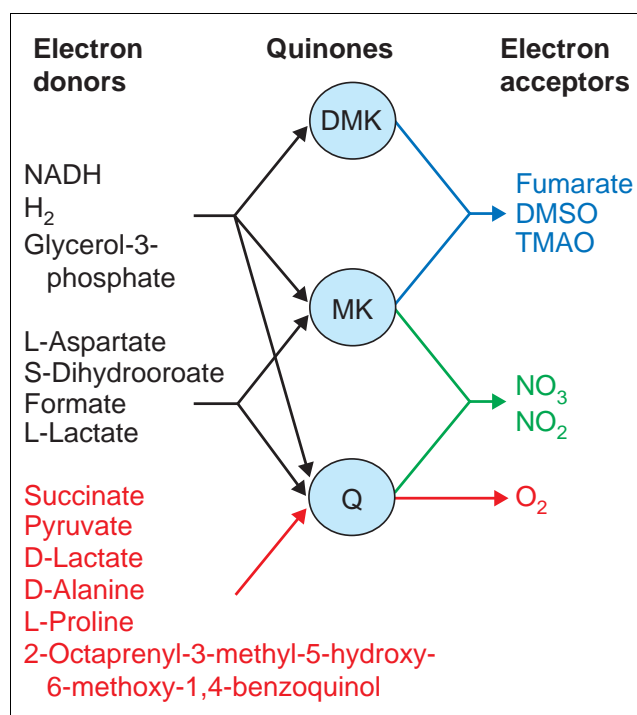
All of these reactions are elementally balanced but not charge balanced (see Additional data file for definition of metabolite abbreviations).

determine the charge associated with the ion complex. The biomass reaction [8], representing the drain of biosynthetic constituents from the network and the growth-associated ATP requirement, was also changed to include internal protons and water. The amount of water needed in the biomass reaction is equal to the amount of ATP hydrolyzed to meet the growth-associated ATP requirement. The hydrolysis of ATP results in the production of a proton while the utilization of NADPH and NADH consumes a proton; this results in the net production of protons in the biomass reaction.

Other updates to the *iJE660a* reaction network are also notable. A number of reactions in *iJE660a* could not previously be assigned to an ORF, but are now assigned to an ORF as a result of the updated genome annotation [12], such as *mtn* and *uppS*. Other ORF names have changed and these were also updated. Some of the original model reactions were modified in addition to including internal protons and water. These modifications mainly included changes in the stoichiometric coefficients, cofactor usage and reaction reversibility. In some cases, the metabolites that participate in the reaction were changed. Forty-two reactions were removed from *iJE660a*, and these are listed in the additional data files along with the reasons for their removal.

*iJR904* also accounts for the specificity of the quinones in the individual reactions involved in the electron transport chain (Figure 3). *E. coli* K-12 uses three quinones: ubiquinone (Q), menaquinone (MK) and demethylmenaquinone (DMK) to transfer electrons from the electron donor to the terminal acceptor; in *iJE660a* there was no distinction between the three quinones and they were all treated as ubiquinone, which led to inaccurate electron donor/electron acceptor pairs.

GPR associations are for the first time directly included in the *iJR904* model, and examples of some are shown in Figure 2. GPR associations have been constructed and their images can be found in the additional data files. These GPR associations can be used to evaluate the reactions remaining in the

**Figure 3**

Quinone specificity for electron donors and terminal acceptors. *E. coli* *iJR904* also accounts for the quinone specificity of different reactions. Electron donors are listed on the left, terminal electron acceptors are on the right, and the three types of quinones (DMK, MK, Q; note that these abbreviations differ from those listed in the additional data files) that serve as carriers are shown in the middle. The electron donors shown in red were unable to donate their electrons to fumarate in *iJE660a*, but are now unable to do so. DMK, demethylmenaquinone; DMSO, dimethyl sulfoxide; MK, menaquinone; Q, ubiquinone; TMAO, trimethylamine N-oxide.

metabolic network after deletion of a specific gene. Including these associations directly into *iJR904* will lead to a more accurate assessment of the effects of gene deletions. In addition, these GPR associations are necessary for analyzing diverse datasets by the model and using these datasets to further identify physiological states.

Thus, *iJR904* accounts more accurately for a number of the metabolic processes in *E. coli* K-12 MG1655, and expands in scope significantly through the addition of GPR associations. *E. coli* *iJR904* GSM/GPR is no longer a purely metabolic model.

### Systemic properties

A list of network components alone does not explain how the components work together to produce a biological function. These systemic properties can only be investigated when considering all the components simultaneously; it is the interaction of these components that provides the most information about cellular behavior. As with *iJE660a*, a myriad of other

issues can be addressed with *iJR904*. We will address three types of issues in this paper using *iJR904*: gap analysis and putative ORF assignments, the importance of global proton balancing, and phase plane analysis [16].

#### *Identification and resolution of dead ends*

A 'dead end' exists in a metabolic network if a metabolite is either only produced or only consumed in the network. If a metabolic network contains a gap, it is missing the biochemical reactions that can produce or consume the dead end metabolites. *iJR904* has 70 dead end metabolites or gaps in the network; these are listed in the additional data files. These 70 metabolites participate in 89 reactions, indicating that at least 89 model reactions can never be used if the network is to operate at steady state. The reactions that lead up to the dead ends in *iJR904* are included so that when the gaps are filled in at a future date, the network will be fully functional. Some of these network gaps could be reconciled by the addition of transporters, while others could be reconciled by modifying the growth function, that is, including dead end metabolites as requirements for biomass production. Neither of these steps was taken here since genomic or biochemical evidence could not be found to support their inclusion.

Using these gaps, we attempted to identify new functional assignments based on sequence homology searches. A list of EC numbers corresponding to enzymes (not included in the model) that could resolve the gaps, was generated. This list was pooled together with the enzymes known to occur in *E. coli* which lack assigned loci (EcoCyc [14]). We subsequently collected amino acid sequences from other organisms (orthologous sequences) assigned to these enzymatic functions for a homology search study.

A total of 83 training sets, each with an average of 11 orthologous sequences, was collected and compared against the *E. coli* genome. Each training set includes multiple orthologous sequences that correspond to an enzyme of interest. Of the 83 training sets, 61 are for enzymes which connect to gaps in the existing network and the remaining 22 are for some of the enzymes listed in EcoCyc. Each training set was processed using the alignment programs MEME [17] and ClustalW [18] to generate a profile for the corresponding enzyme. Using these profiles MAST [19] and HMMER [20] were used to identify similar ORFs in the *E. coli* genome. Of the 61 enzymes that could resolve network gaps, we assigned putative loci for 12 of them. In addition, putative loci could be found for 15 of the 22 enzymes listed in EcoCyc. Some of these enzymes have multiple matches within the *E. coli* genome, which together resulted in 55 putative assignments.

These results were inspected manually and found to be relevant and consistent across the three search methods (MAST, with and without end-gap penalty, and HMMER). The results of this study largely coincided with the annotation performed by Serres *et al.* [12]; however, most annotation updates added

more specificity to the type of reactions the enzymes were predicted to catalyze and, in some cases, suggested additional substrates that known enzymes might act upon (Table 2). Table 2 lists the top three matches for each enzyme (except for the case when the match is a known isozyme); a complete list of all results and expected values (e-values) can be found in the additional data files. The putative assignments presented in Table 2 should be used with care. For example, there are multiple putative assignments for the acyl-CoA dehydrogenase enzyme for which the gene has recently been found [21], but the actual gene locus for this enzyme (b0221) does not have the most significant e-value among the list of potential loci.

#### *Effects of constraining proton exchange flux*

The importance of balancing protons internally can now be investigated with *iJR904* since the metabolic network accounts for all the protons being generated and consumed by the individual metabolic and transport reactions (only external protons associated with the proton motive force were accounted for in *iJE660a*). The medium can serve as a pool both supplying and dissipating external protons as needed by the cell. During growth on some carbon sources, the generation of internal protons by the metabolic reactions is relieved by secreting protons into the medium. This subsequently reduces the amount of ATP made by ATPase since these protons could be used to drive this reaction. Under other conditions, a shortage of internal protons is compensated for by taking up protons from the medium and transporting them across the cell membrane into the cytosol.

The effects that the exchange of protons across the system boundary have on predicted growth rates were investigated. A robustness analysis [22], in which the flux through the proton exchange reaction was constrained from its optimal value down to zero, was performed under aerobic conditions for a variety of carbon sources (Figure 4). The predicted growth rates for different carbon sources respond differently as the exchange flux of protons (between the cell and the medium) is reduced to zero; glucose and glycerol were the most sensitive to proton exchange while D- and L-lactate were the least sensitive.

When either glucose or glycerol was used as the carbon source, excess protons were generated intracellularly; this excess was relieved by secreting extracellular protons, thereby lowering the pH of the medium. For pyruvate, D- and L-lactate, acetate,  $\alpha$ -ketoglutarate ( $\alpha$ KG), succinate and malate there is a shortage of internal protons; as a result, cells would uptake protons from the medium thereby raising the pH. Since there can be no net accumulation of charge within the system, the total charge entering the system must equal the charge leaving the system. Pyruvate, lactate, acetate,  $\alpha$ -ketoglutarate, succinate and malate, as used in these simulations, have a negative charge so  $H^+$  must be taken up; however, if the uncharged acidic form of these compounds

**Table 2****List of ORFs in *E. coli* with updated annotations based on sequence similarity**

| EC number                          | Bnum         | Gene                | Published annotation [12]   | Suggested annotation                                 |
|------------------------------------|--------------|---------------------|---|--|
| <b>1.1.1.48</b>                    | <b>b1315</b> | <b><i>ycjS</i></b>  | <b>Putative NADH-dependent dehydrogenase</b>  | <b>D-Galactose 1-dehydrogenase</b>                   |
| <b>1.1.1.48</b>                    | <b>b1624</b> | <b><i>ydgj</i></b>  | <b>Putative NAD(P)-binding dehydrogenase</b>  | <b>D-Galactose 1-dehydrogenase</b>                   |
| <b>1.1.1.48</b>                    | <b>b3440</b> | <b><i>yhhX</i></b>  | <b>Putative NAD(P)-binding dehydrogenase</b>  | <b>D-Galactose 1-dehydrogenase</b>                   |
| 1.1.1.5                            | b2426        | <i>ucpA</i>         | Putative oxidoreductase, NAD(P)-binding   | Acetoin dehydrogenase, diacetyl reductase            |
| 1.1.1.5                            | b2137        | <i>yohF</i>         | Putative oxidoreductase   | Acetoin dehydrogenase, diacetyl reductase            |
| 1.1.1.5                            | b4266        | <i>idnO</i>         | 5-Keto-D-gluconate-5-reductase  | Acetoin dehydrogenase, diacetyl reductase            |
| 1.2.1.19                           | b1385        | <i>feaB</i>         | Phenylacetaldehyde dehydrogenase  | Aminobutyraldehyde dehydrogenase                     |
| 1.2.1.19                           | b1444        | <i>ydcW</i>         | Putative aldehyde dehydrogenase   | Aminobutyraldehyde dehydrogenase                     |
| 1.2.1.19                           | b3588        | <i>aldB</i>         | Aldehyde dehydrogenase B (lactaldehyde dehydrogenase)   | Aminobutyraldehyde dehydrogenase                     |
| 1.2.1.24                           | b1385        | <i>feaB</i>         | Phenylacetaldehyde dehydrogenase  | Succinate-semialdehyde dehydrogenase                 |
| 1.2.1.24                           | b1444        | <i>ydcW</i>         | Putative aldehyde dehydrogenase   | Succinate-semialdehyde dehydrogenase                 |
| 1.2.1.24                           | b1415        | <i>aldA</i>         | Aldehyde dehydrogenase A, NAD-linked  | Succinate-semialdehyde dehydrogenase                 |
| 1.2.7.1                            | b1378        | <i>nifj</i>         | Putative pyruvate-flavodoxin oxidoreductase   | Pyruvate synthase                                    |
| <b>1.3.1.2</b>                     | <b>b2146</b> | <b><i>yeiT</i></b>  | <b>Putative glutamate synthase</b>  | <b>Dihydrothymine dehydrogenase</b>                  |
| <b>1.3.1.2</b>                     | <b>b2147</b> | <b><i>yeiA</i></b>  | <b>Putative dihydropyrimidine dehydrogenase, FMN-linked</b>   | <b>Dihydrothymine dehydrogenase</b>                  |
| <b>1.3.1.2</b>                     | <b>b2878</b> | <b><i>b2878</i></b> | <b>Putative oxidoreductase</b>  | <b>Dihydrothymine dehydrogenase</b>                  |
| 1.3.99.3                           | b1695        | <i>ydiO</i>         | Putative acyl-CoA dehydrogenase   | Acyl-CoA dehydrogenase                               |
| 1.3.99.3                           | b0039        | <i>caiA</i>         | Putative acyl-CoA dehydrogenase, carnitine metabolism   | Acyl-CoA dehydrogenase                               |
| 1.3.99.3                           | b4187        | <i>aidB</i>         | Putative acyl-CoA dehydrogenase; adaptive response (transcription activated by Ada)                                   | Acyl-CoA dehydrogenase                               |
| 1.6.6.9                            | b3551        | <i>bisC</i>         | Biotin sulfoxide reductase  | Trimethylamine-N-oxide reductase (TMAO reductase II) |
| 1.6.6.9                            | b1587        | <i>b1587</i>        | Putative reductase  | Trimethylamine-N-oxide reductase (TMAO reductase II) |
| 1.6.6.9                            | b1588        | <i>b1588</i>        | Putative reductase  | Trimethylamine-N-oxide reductase (TMAO reductase II) |
| 1.6.99.2                           | b0046        | <i>yabF</i>         | Putative electron transfer flavoprotein-NAD/FAD/quinone oxidoreductase, subunit for KefC K <sup>+</sup> efflux system | NAD(P)H dehydrogenase                                |
| 1.6.99.2                           | b3351        | <i>yheR</i>         | Putative electron transfer flavoprotein-NAD/FAD/quinone oxidoreductase  | NAD(P)H dehydrogenase                                |
| 1.6.99.2                           | b0901        | <i>ycaK</i>         | Putative electron transfer flavoprotein-NAD/FAD/quinone oxidoreductase  | NAD(P)H dehydrogenase                                |
| <b>2.3.3.11 (formerly 4.1.3.9)</b> | <b>b2264</b> | <b><i>menD</i></b>  | <b>Bifunctional modular MenD: 2-oxoglutarate decarboxylase and SHCHC synthase</b>                                     | <b>2-Hydroxyglutarate synthase</b>                   |
| <b>2.3.3.11 (formerly 4.1.3.9)</b> | <b>b3671</b> | <b><i>ilvB</i></b>  | <b>Acetolactate synthase I, large subunit, valine-sensitive, FAD and thiamine PPI binding</b>                         | <b>2-Hydroxyglutarate synthase</b>                   |
| 2.7.1.23                           | b2615        | <i>yfjB</i>         | Conserved protein   | NAD <sup>+</sup> kinase                              |
| 2.7.1.23                           | b3916        | <i>pfkA</i>         | 6-phosphofructokinase I   | NAD <sup>+</sup> kinase                              |
| 2.7.2.1                            | b3115        | <i>tdcD</i>         | Propionate kinase/acetate kinase II, anaerobic  | Acetate kinase (ackB)                                |
| <b>2.7.8.2</b>                     | <b>b1408</b> | <b><i>b1408</i></b> | <b>Putative enzyme</b>  | <b>Diaclyglycerol cholinephosphotransferase</b>      |
| 2.8.1.2                            | b2521        | <i>sseA</i>         | Putative sulfurtransferase  | 3-Mercaptopyruvate sulfurtransferase                 |
| 2.8.1.2                            | b1757        | <i>ynjE</i>         | Putative thiosulfate sulfur transferase   | 3-Mercaptopyruvate sulfurtransferase                 |
| 2.8.3.8                            | b2222        | <i>atoA</i>         | Acetyl-CoA:acetoacetyl-CoA transferase, beta subunit  | Acetate CoA-transferase                              |
| 2.8.3.8                            | b2221        | <i>atoD</i>         | Acetyl-CoA:acetoacetyl-CoA transferase, alpha subunit   | Acetate CoA-transferase                              |
| 2.8.3.8                            | b1694        | <i>ydiF</i>         | Putative acetyl-CoA:acetoacetyl-CoA transferase alpha subunit   | Acetate CoA-transferase                              |
| 3.1.1.31                           | b0678        | <i>nagB</i>         | Glucosamine-6-phosphate deaminase   | 6-Phosphogluconolactonase (Pgl)                      |
| 3.1.1.31                           | b3718        | <i>yieK</i>         | Putative isomerase  | 6-Phosphogluconolactonase (Pgl)                      |

**Table 2** (Continued)**List of ORFs in *E. coli* with updated annotations based on sequence similarity**

|                 |              |                    |  |   |
|-----------------|--------------|--------------------|--|---|
| 3.1.1.31        | b3141        | <i>agal</i>        | Putative galactosamine-6-phosphate isomerase   | 6-Phosphogluconolactonase (Pgl)                                       |
| 3.2.1.68        | b3431        | <i>glgX</i>        | Glycosyl hydrolase   | Isoamylase  |
| 3.5.1.2         | b1524        | <i>yneH</i>        | Putative glutaminase   | Glutaminase A or B  |
| 3.5.1.2         | b0485        | <i>ybaS</i>        | Putative glutaminase   | Glutaminase A or B  |
| <b>3.6.1.19</b> | <b>b2954</b> | <b><i>yggV</i></b> | <b>Conserved hypothetical protein</b>  | <b>Nucleoside-triphosphate (ITP) diphosphatase</b>                    |
| 3.6.1.22        | b3996        | <i>yjaD</i>        | Conserved hypothetical protein, MutT-like protein  | NAD <sup>+</sup> diphosphatase  |
| <b>3.6.1.5</b>  | <b>b3615</b> | <b><i>yibD</i></b> | <b>Putative glycosyltransferase</b>  | <b>Inosine triphosphate diphosphatase</b>                             |
| <b>3.6.1.6</b>  | <b>b3614</b> | <b><i>yibQ</i></b> | <b>Conserved hypothetical protein</b>  | <b>Nucleoside (IDP) diphosphatase</b>                                 |
| <b>4.1.1.39</b> | <b>b3615</b> | <b><i>yibD</i></b> | <b>Putative glycosyltransferase</b>  | <b>Ribulose-bisphosphate carboxylase (2-phosphoglycolate forming)</b> |
| <b>4.1.2.10</b> | <b>b0311</b> | <b><i>betA</i></b> | <b>Choline dehydrogenase, a flavoprotein</b>   | <b>Hydroxynitrile lyase</b>   |
| <b>4.1.2.10</b> | <b>b3168</b> | <b><i>infB</i></b> | <b>Protein chain initiation factor IF-2</b>  | <b>Hydroxynitrile lyase</b>   |
| <b>4.2.1.66</b> | <b>b3022</b> | <b><i>ygiU</i></b> | <b>Conserved protein</b>   | <b>Cyanide hydratase</b>  |
| <b>6.2.1.12</b> | <b>b4069</b> | <b><i>acs</i></b>  | <b>Acetyl-CoA synthetase</b>   | <b>Hydroxycinnamate-CoA ligase</b>                                    |
| <b>6.2.1.12</b> | <b>b1701</b> | <b><i>ydiD</i></b> | <b>Putative CoA-dependent ligase</b>   | <b>Hydroxycinnamate-CoA ligase</b>                                    |
| <b>6.2.1.12</b> | <b>b2836</b> | <b><i>aas</i></b>  | <b>bifunctional multimodular Aas: 2-acylglycerophospho-ethanolamine acyl transferase</b> | <b>Hydroxycinnamate-CoA ligase</b>                                    |
| <b>6.2.1.4</b>  | <b>b0728</b> | <b><i>sucC</i></b> | <b>Succinyl-CoA synthetase, beta subunit</b>   | <b>Succinate-CoA ligase (ITP forming)</b>                             |
| <b>6.2.1.4</b>  | <b>b0729</b> | <b><i>sucD</i></b> | <b>Succinyl-CoA synthetase, alpha subunit, NAD(P) binding</b>                            | <b>Succinate-CoA ligase (ITP forming)</b>                             |

Annotations shown in bold arose from analyzing the network gaps in *iJR904*.

was used instead (and the acid-base reaction was included in the network - generating proton(s) and the basic form of the compound) it would be predicted that H<sup>+</sup> would be secreted by the cell thereby lowering the pH.

It is generally thought that the pH of the medium becomes more acidic as *E. coli* grows. A lowering of pH has been observed for growth on unbuffered medium with glycerol; however, during growth on unbuffered medium with disodium succinate or sodium acetate the medium becomes more basic (J.L.R. and B.O.P., unpublished data). Clearly *iJR904* with charge-balanced reactions highlights the challenge that cells have with globally balancing protons. As a part of the iterative model building process [2] *iJR904* can be used to design informative experiments to systematically address this issue.

#### Phenotypic phase plane (PhPP) comparisons

The phenotypic phase planes [16] for growth on different carbon sources were calculated using both models *iJR904* and *iJE660a*. A description of phenotypic phase planes can be found in Materials and methods. For these simulations the carbon uptake rate and oxygen uptake rate were varied. The carbon substrates tested included: glucose, pyruvate, acetate, glycerol, D-lactate,  $\alpha$ KG, succinate and malate. The phase planes for pyruvate, D-lactate and succinate calculated using

*iJR904* were nearly identical to those calculated with model *iJE660a* (the lines demarcating the different phases only moved slightly). These results show that the modified and new reactions contained in *iJR904* did not significantly affect the phase planes for these substrates, indicating that *iJR904* makes similar predictions regarding optimal growth on these substrates.

The line of optimality (LO) on a phenotypic phase plane corresponds to the conditions (oxygen and substrate uptake rates) which can maximize the biomass yield. The largest shifts in the line of optimality were observed for growth on pyruvate and  $\alpha$ KG. However, these shifts are relatively small indicating that the optimal oxygen uptake and carbon source uptake rates needed to generate the maximal amount of biomass do not change significantly (less than 10%).

The phenotypic phase planes for carbon sources other than pyruvate, D-lactate, and succinate have more significant changes when calculated with *iJR904* as compared to *iJE660a*. These include growth on the following carbon sources: glycerol, glucose, acetate, malate and  $\alpha$ KG. The resulting phase planes calculated using *iJR904* and *iJE660a* are shown in red and blue, respectively, in Figure 5a-e. For the malate and glucose phase planes (Figure 5a,b) one of the lines only appears on the phase plane calculated using



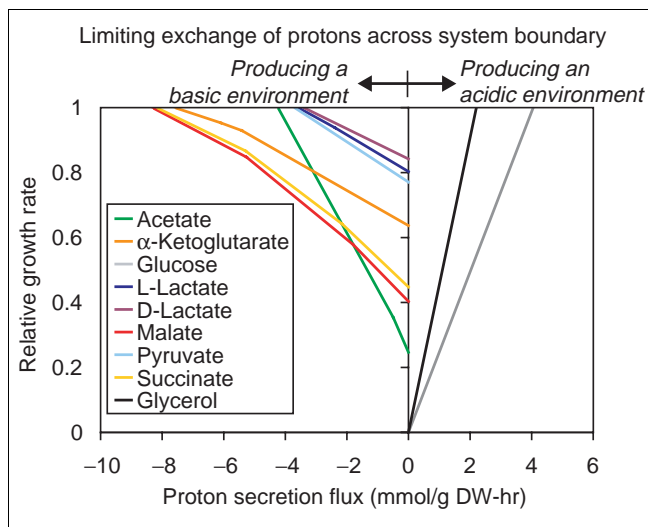


**Figure 4**

Effect of proton balancing on predicted growth rate. The figure shows how limiting the exchange of protons between the cell and the medium affects the predicted growth rates under aerobic conditions. The relative growth rate (y-axis) is the ratio of the predicted growth rate when the proton exchange flux is limited over the predicted growth rate when the proton exchange flux is not limited (at its optimal value). These calculations are for the conditions of aerobic growth on minimal media; the carbon source uptake rates were set to 5 mmol/g DW-hr and the maximum oxygen uptake rate was set to 20 mmol/g DW-hr. Carbon sources resulting in an outward flux of protons (lines to the right of the y-axis) would make the medium more acidic, while carbon sources resulting in an inward flux of protons (lines to the left of the y-axis) would make the medium more basic.

*iJE660a*; these changes are attributed to the effects of global proton balancing described in the previous section. This issue also accounts for changes in the acetate phase plane (Figure 5c) and is a contributing factor to the changes observed with the glycerol and  $\alpha$ KG phase planes. However, other changes (discussed below) to the metabolic networks have more significant effects on these two phase planes.

#### Glycerol phase plane

The changes in the glycerol phenotypic phase plane (Figure 5d) were less drastic than those for the  $\alpha$ KG phase plane (Figure 5e, see comments below). The only major change was that the lines in the microaerobic region shifted downward. This change is a result of the removal of two reactions involved in pyridoxal recycling which were previously assigned to *pdxH*. The two reactions are not included in the metabolic network defined by *iJR904* for reasons explained in the additional data files.

#### $\alpha$ -Ketoglutarate phase plane

The two-dimensional phenotypic phase plane for  $\alpha$ KG is noticeably different when calculated for *iJR904* and *iJE660a* (Figure 5e). One notable feature is that *iJR904* predicts completely anaerobic growth on  $\alpha$ KG, while *iJE660a* predicts that

oxygen is required for growth on  $\alpha$ KG. Under oxygen limitations, corresponding to regions below the line of optimality, the expanded model is also more efficient at producing biomass from  $\alpha$ KG than the previous model. As oxygen becomes more limiting, *iJR904* becomes increasingly more efficient at generating biomass than *iJE660a*.

Examination of the calculated optimal flux distributions provides insights into why *iJR904* is more efficient. One of the reasons for this increased growth efficiency is that *iJR904* includes the citrate lyase enzyme, which converts citrate (CIT) to acetate (AC) and oxaloacetate (OAA). During oxygen-limited growth, *iJR904* predicts that some of the  $\alpha$ KG is converted to OAA by first reversing some of the TCA cycle reactions to generate CIT and then splitting CIT into AC and OAA by citrate lyase. The rest of the  $\alpha$ KG is consumed through the forward reactions of the TCA cycle to produce malate (Figure 6). Removal of the citrate lyase reaction from the network under anaerobic conditions shows two other, less-efficient routes that would still enable *iJR904* to predict anaerobic growth. These new metabolic routes, which are dependent on at least one of the new additions, are depicted in Figure 5f.

## Conclusions

This paper reports the curation and expansion of a previous genome-scale constraint-based model of *E. coli* metabolism (*iJE660a* GSM) that is now used in multiple laboratories (A.L. Barabasi, personal communication; Church and colleagues [23]; H. Greenberg, personal communication and C. Maranas, personal communication). This expanded model, *iJR904* GSM/GPR, includes 37% more metabolic genes and 47% more metabolic reactions. Each reaction in the network is now both elementally and charge balanced with the exception of the six reactions listed in Table 1. While the new reactions added to the network do not change many of the predicted optimal phenotypes, there are instances in which the expanded model makes significantly different predictions, examples of which occur when glycerol, glucose, malate, acetate and  $\alpha$ KG are used as the carbon sources under oxygen-limited conditions.

The analysis of dead ends or gaps in the network has led to putative annotations of 55 ORFs. If these putative functional assignments are verified biochemically they can be included in future updates of *iJR904*. Ideally an iterative process will be developed, within which the model can help identify new targets, and, if verified, can lead to an updated model. This iterative process [2] would be likely to produce more useful results in less-characterized organisms and has already been successful in helping to identify malate dehydrogenase in *Helicobacter pylori* [24] and citrate synthase in *Geobacter sulfurreducens* (D. Lovley, unpublished results).

The incorporation of GPR associations into *iJR904* will allow for the analysis of transcriptomic and proteomic data



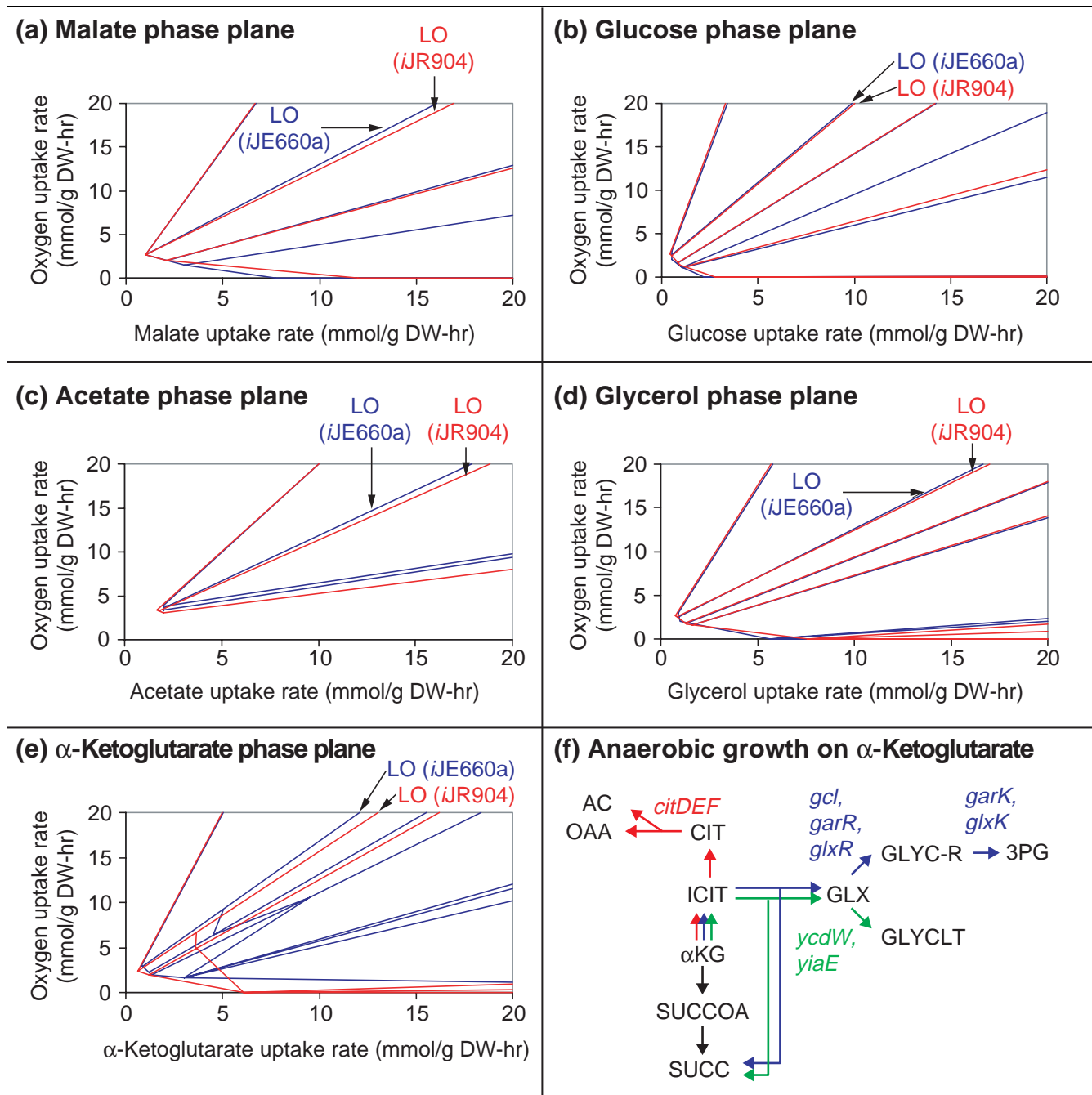


**Figure 5**  
 Comparisons between phenotypic phase planes (PhPP) calculated using iJR904 and iJE660a. **(a-e)** The PhPP for growth on (a) malate, (b) glucose, (c) acetate, (d) glycerol, and (e)  $\alpha$ -ketoglutarate ( $\alpha$ KG) are shown, where the red lines show the PhPP calculated from iJR904 and the blue lines the PhPP calculated from iJE660a. The line of optimality (LO) corresponds to maximal biomass yield. **(e)** With  $\alpha$ KG as the carbon source, the phase planes calculated from iJR904 (red line) and iJE660a (blue line) are drastically different in the oxygen-limited region (area below the LO). **(f)** The different metabolic routes (along with their associated genes) added to the network in iJR904 that enable fermentative growth on  $\alpha$ KG are shown in red, blue and green. AC, acetate; CIT, citrate; GLYCLT, glycolate; GLYC-R, R-glycerate; GLX, glyoxylate; ICIT, isocitrate;  $\alpha$ KG,  $\alpha$ -ketoglutarate, OAA, oxaloacetate; 3PG, 3-phospho-D-glycerate; SUCC, succinate; SUCCOAc, succinyl-CoA.

directly; it also enables the incorporation of these datasets to further constrain the solution space leading to more accurate

predictions of phenotypic data. *E. coli* iJR904 can now serve as a model centric database which could analyze and reconcile

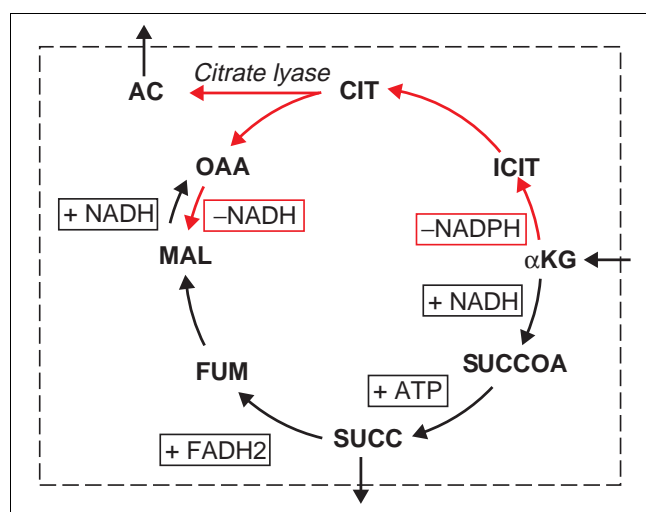


**Figure 6**

Flux map of TCA cycle and citrate lyase. During oxygen-limited growth on  $\alpha$ KG maximal biomass will be made by utilizing the citrate lyase reaction. As oxygen becomes more limiting, the reactions shown in red, culminating in the production of oxaloacetate (OAA), were predicted by *iJR904* to be used more heavily than the forward direction of the TCA cycle reactions (shown in black). *iJE660a* does not include the citrate lyase reaction so carbon flow is directed only in the forward direction of the TCA cycle; these reactions produce more reduced redox carriers, which are difficult for the cell to oxidize in an oxygen-limited environment. The '+' sign indicates that the cofactor is produced by the reaction in the direction shown and the '-' sign indicates that the cofactor is consumed. For abbreviations see Figure 5, with the following additions: ACCoA, acetyl-CoA; FUM, fumarate; MAL, malate, PYR, pyruvate.

heterogeneous datasets as well as use these datasets to aid in model predictions.

## Materials and methods

### Constraint-based modeling

A stoichiometric matrix,  $\mathbf{S}$  ( $m \times n$ ), is constructed where  $m$  is the number of metabolites and  $n$  the number of reactions. Each column of  $\mathbf{S}$  specifies the stoichiometry of the metabolites in a given reaction from the metabolic network. Mass balance equations can be written for each metabolite by taking the dot product of a row in  $\mathbf{S}$ , corresponding to a particular metabolite, and a vector,  $\mathbf{v}$ , containing the values of the fluxes through all reactions in the network. A system of mass balance equations for all the metabolites can be represented as follows:

$$\frac{d\mathbf{X}}{dt} = \mathbf{S} \cdot \mathbf{v} \quad (1)$$

where  $\mathbf{X}$  is a concentration vector of length  $m$ , and  $\mathbf{v}$  is a flux vector of length  $n$ . At steady-state, the time derivatives of metabolite concentrations are zero, and equation (1) can be simplified to:

$$\mathbf{S} \cdot \mathbf{v} = 0$$

It follows that in order for a flux vector  $\mathbf{v}$  to satisfy this relationship, the rate of production must equal the rate of consumption for each metabolite. Application of additional constraints further reduces the number of allowable flux distributions,  $\mathbf{v}$ .

Limits on the range of individual flux values can further reduce the number of allowable solutions. These constraints have the form:

$$\alpha \leq v_i \leq \beta$$

where  $\alpha$  and  $\beta$  are the lower and upper limits, respectively. Maximum flux values ( $\beta$ ) can be estimated based on enzymatic capacity limitations or, for the case of exchange reactions, measured maximal uptake rates can be used. Thermodynamic constraints, regarding the reversibility or irreversibility of a reaction, can be applied by setting the  $\alpha$  for the corresponding flux to zero if the reaction is irreversible.

These constraints are not sufficient to shrink the original solution space to a single solution. Instead a number of solutions remain which make up the allowable solution space. Linear optimization can be used to find the solution that maximizes a particular objective function. Some examples of objective functions include the production of ATP, NADH, NADPH or a particular metabolite. An objective function with a combination of the metabolic precursors, energy and redox potential required for the production of biomass has proven useful in predicting *in vivo* cellular behavior [9,10,25,26].

### Simulation conditions

Simulations with *iJR904* were all done using the software package SimPheny™ (Genomatica, San Diego, CA); this software was also used to build *iJR904*. All calculations were made using the conditions outlined in this section. The biomass reaction was the same as that reported previously [8] with the addition of intracellular protons and water, and can be found in the additional data files. All flux values reported in this section are in units of mmol/g DW-hr. The flux through the non-growth associated ATP maintenance reaction (ATPM in the additional data files) was fixed to 7.6. Fluxes through all other internal reactions have an upper limit of  $1 \times 10^{30}$ ; if the reaction is reversible the lower limit is  $-1 \times 10^{30}$  and if it is irreversible the lower limit is zero.

In addition to the metabolic reactions listed in the additional data files, reversible exchange reactions for all external metabolites were also included in the simulations to allow external metabolites to cross the system boundaries. If these exchange reactions are used in the forward direction the external metabolites leave the system and if used in the reverse direction (that is, a negative flux value through the reaction) the external metabolites enter the system.

The following external metabolites were allowed to freely enter and leave the system: ammonia, water, phosphate, sulfate, potassium, sodium, iron (II), carbon dioxide and protons (except during the robustness study where proton exchange flux was constrained down to zero). The corresponding exchange fluxes for these metabolites have a lower and upper flux limit of  $-1 \times 10^{30}$  and  $1 \times 10^{30}$ , respectively. Aerobic conditions were simulated with a maximum oxygen uptake rate of 20 mmol/g DW-hr, by setting the lower and upper limits for the oxygen exchange flux to -20 and 0 respectively, and anaerobic conditions were simulated by fixing the oxygen uptake rate to 0. All other external metabolites, except for the carbon source, were only allowed to leave the system. The lower and upper limits on their corresponding exchange fluxes were 0 and  $1 \times 10^{30}$ , respectively. Growth on different carbon sources was simulated by allowing those external metabolites to enter the system; the actual flux values for uptake rates used in the simulations are noted in the text and figures, where the upper limit is 0 and the lower limit is the negative of the uptake rate listed. These constraints are also summarized in the additional data files.

### Phenotypic phase planes (PhPP)

Phenotypic phase plane analysis was developed to generate a global view of the optimality properties of a network [16]. The phenotypic phase plane is constructed from a large number of individual optimal solutions and gives an overall view of the optimality properties of the network. PhPPs are used to show all possible quantitative flux distributions through a network while varying two or three constrained fluxes. The different regions of the phase plane have qualitatively different flux distributions that translate to different metabolic phenotypes. One important feature of the PhPP is the line of optimality (LO). Points that lie on the LO optimize the objective function for a given substrate uptake rate. When the cell is operating along the LO, calculated when the growth rate is used as the objective function, the cell is growing with a maximal biomass yield.

### Identification of dead ends

Dead end metabolites are classified as such if a metabolite can either be produced but not consumed or consumed but not produced. By examining the connectivity of the metabolites in the **S** matrix, a list of dead ends can be generated. Once these are identified, the number of reactions directly involved with these metabolites can be determined by enumerating the number of non-zero elements in the row corresponding to each dead end metabolite.

### Sequence annotations

A list of reactions and associated enzymes that could connect the dead ends with the rest of the network was gathered from LIGAND (Database of Chemical Compounds and Reactions in Biological Pathways [13]). These are enzymes known to act on those metabolites in other organisms. The enzymes listed in EcoCyc which are known to be in *E. coli* but lack assigned

loci, were also added to the search list. The enzyme commission numbers for this combined list of enzymes were used in queries against the SwissProt, TremBl and TremBlnew databanks (using Sequence Retrieval System [27]) to retrieve the enzymes' corresponding amino acid sequences. Known orthologous sequences of all of the enzymes of interest were grouped together to construct multiple sequence alignments. Two separate programs, MEME (Multiple Expectation maximization for Motifs Elicitation [17]) and ClustalW [18] were used for this purpose. MEME was run assuming that each sequence may contain a variable number of non-overlapping occurrences of each motif and up to three distinct motifs. Each training set was processed twice with MEME, once with the program's default end-gap penalty and once without it. Default values were used for gap-opening penalty and gap-extension penalty. All sequences in each training set were weighed equally by MEME. ClustalW, however, down-weighted similar sequences in proportion to their degree of relatedness. Pair-wise alignments in ClustalW were run with a dynamic programming algorithm (slow option) and with the Reset Gap option off.

The MEME output files were submitted to MAST [19] (Motif Alignment and Search Tool, version 3.0 online) and searched for matching sequences against the *E. coli* genome. MAST returned a list of high-scoring sequences and their annotations. ClustalW output files were used by HMMER's *hmmbuild* and *hmmcalibrate* (version 2.2g [20]) with default parameters to train profile HMMs (Hidden Markov Models). *hmmsearch* was subsequently applied to find sequences in the *E. coli* genome that matched each profile. Results from MAST's and HMMER's searches were manually examined, and relevant matches were reported.

### Additional data files

The additional data consists of three files. The Excel file (Additional data file 1) contains the following: a list of the reactions in *iJR904*; definitions of the metabolite abbreviations; a list of the exchange fluxes used in simulations and their constraints; a list of the dead end metabolites in the metabolic network; a list of the reactions that were not included from *iJE660a* and a complete list of the sequence comparison results (including e-values). A zip file (Additional data file 2) is also provided, including the JPEG images of all the GPR associations and a detailed document describing how to interpret these images. The GPR image files are each labeled to correspond to either an individual gene or reaction. The third file (Additional data file 3) contains six maps of metabolism which together include all the reactions in *iJR904*; the reaction and metabolite abbreviations are the same as those listed in the Excel file.

### Acknowledgements

The authors would like to thank Markus Herrgard for his advice regarding sequence comparisons, Evelyn Travnik for her help putting together the

additional data files, as well as Timothy Allen, Jason Papin and Sharon Wiback for their comments on the manuscript. Support for this work was provided by the NIH (grants GM57092 and GM62791) and the San Diego Fellowship to T.V.

## References

1. Palsson BO: **In silico biology through "omics"**. *Nat Biotechnol* 2002, **20**:649-650.
2. Palsson BO: **The challenges of in silico biology**. *Nat Biotechnol* 2000, **18**:1147-1150.
3. Edwards JS, Covert M, Palsson B: **Metabolic modelling of microbes: the flux-balance approach**. *Environ Microbiol* 2002, **4**:133-140.
4. Varma A, Palsson BO: **Metabolic flux balancing: basic concepts, scientific and practical use**. *BioTechnology* 1994, **12**:994-998.
5. Bonarius HPJ, Schmid G, Tramper J: **Flux analysis of underdetermined metabolic networks: the quest for the missing constraints**. *Trends Biotechnol* 1997, **15**:308-314.
6. Price ND, Papin JA, Schilling CH, Palsson BO: **Genome-scale microbial in silico models: the constraints-based approach**. *Trends Biotechnol* 2003, **21**:162-169.
7. Reed JL, Palsson BO: **Thirteen years of building constraint-based in silico models of Escherichia coli**. *J Bacteriol* 2003, **185**:2692-2699.
8. Edwards JS, Palsson BO: **The Escherichia coli MGI655 in silico metabolic genotype: its definition, characteristics, and capabilities**. *Proc Natl Acad Sci USA* 2000, **97**:5528-5533.
9. Edwards JS, Ibarra RU, Palsson BO: **In silico predictions of Escherichia coli metabolic capabilities are consistent with experimental data**. *Nat Biotechnol* 2001, **19**:125-130.
10. Ibarra RU, Edwards JS, Palsson BO: **Escherichia coli K-12 undergoes adaptive evolution to achieve in silico predicted optimal growth**. *Nature* 2002, **420**:186-189.
11. **Systems Biology Research Group** [<http://systemsbiology.ucsd.edu/organisms/ecoli.html>]
12. Serres MH, Gopal S, Nahum LA, Liang P, Gaasterland T, Riley M: **A functional update of the Escherichia coli K-12 genome**. *Genome Biol* 2001, **2**:research0035-0035.7.
13. Goto S, Okuno Y, Hattori M, Nishioka T, Kanehisa M: **LIGAND: database of chemical compounds and reactions in biological pathways**. *Nucleic Acids Res* 2002, **30**:402-404.
14. Karp PD, Riley M, Saier M, Paulsen IT, Collado-Vides J, Paley SM, Pellegrini-Toole A, Bonavides C, Gama-Castro S: **The EcoCyc database**. *Nucleic Acids Res* 2002, **30**:56-58.
15. **TC-DB: Transport Protein Database** [<http://tcdb.ucsd.edu/tcdb/background.php>]
16. Edwards JS, Ramakrishna R, Palsson BO: **Characterizing the metabolic phenotype: a phenotype phase plane analysis**. *Biotechnol Bioeng* 2002, **77**:27-36.
17. Bailey TL, Elkan C: **Fitting a mixture model by expectation maximization to discover motifs in biopolymers**. *Proc Int Conf Intell Syst Mol Biol* 1994, **2**:28-36.
18. Thompson JD, Higgins DG, Gibson TJ: **CLUSTAL W: improving the sensitivity of progressive multiple sequence alignment through sequence weighting, position-specific gap penalties and weight matrix choice**. *Nucleic Acids Res* 1994, **22**:4673-4680.
19. Bailey TL, Gribskov M: **Combining evidence using p-values: application to sequence homology searches**. *Bioinformatics* 1998, **14**:48-54.
20. **HMMER: Profile HMMs for protein sequence analysis** [<http://hmmer.wustl.edu>]
21. Campbell JW, Cronan JE Jr: **The enigmatic Escherichia coli fadE gene is yafH**. *J Bacteriol* 2002, **184**:3759-3764.
22. Edwards JS, Palsson BO: **Robustness analysis of the Escherichia coli metabolic network**. *Biotechnol Prog* 2000, **16**:927-939.
23. Segre D, Vitkup D, Church GM: **Analysis of optimality in natural and perturbed metabolic networks**. *Proc Natl Acad Sci USA* 2002, **99**:15112-15117.
24. Covert MV, Schilling CH, Famili I, Edwards JS, Goryanin II, Selkov E, Palsson BO: **Metabolic modeling of microbial strains in silico**. *Trends Biochem Sci* 2001, **26**:179-186.
25. Varma A, Palsson BO: **Stoichiometric flux balance models quantitatively predict growth and metabolic by-product secretion in wild-type Escherichia coli W3110**. *Appl Environ Microbiol* 1994, **60**:3724-3731.
26. Pramanik J, Keasling JD: **Stoichiometric model of Escherichia coli metabolism: incorporation of growth-rate dependent biomass composition and mechanistic energy requirements**. *Biotechnol Bioeng* 1997, **56**:398-421.
27. Zdobnov EM, Lopez R, Apweiler R, Etzold T: **The EBI SRS server - recent developments**. *Bioinformatics* 2002, **18**:368-373.